



Published in final edited form as:

ACS Chem Biol. 2016 April 15; 11(4): 971–980. doi:10.1021/acscchembio.5b00897.

Expanding the 3-*O*-Sulfate Proteome—Enhanced Binding of Neuropilin-1 to 3-*O*-Sulfated Heparan Sulfate Modulates Its Activity

Bryan E. Thacker^{†,‡}, Emylie Seamen[†], Roger Lawrence[†], Matthew W. Parker[§], Yongmei Xu^{||}, Jian Liu^{||}, Craig W. Vander Kooj[§], and Jeffrey D. Esko^{*,†,‡}

[†]Department of Cellular and Molecular Medicine, Glycobiology Research and Training Center

[‡]Biomedical Sciences Graduate Program, University of California, San Diego, La Jolla, California 92093, United States

[§]Center for Structural Biology, Department of Molecular and Cellular Biochemistry, University of Kentucky, Lexington, Kentucky 40536, United States

^{||}Division of Chemical Biology and Medicinal Chemistry, Eshelman School of Pharmacy, University of North Carolina, Chapel Hill, North Carolina 27599, United States

Abstract

Binding of proteins to heparan sulfate is driven predominantly by electrostatic interactions between positively charged amino acid residues in the protein and negatively charged sulfate groups located at various positions along the polysaccharide chain. Although many heparin/heparan-sulfate-binding proteins have been described, few exhibit preferential binding for heparan sulfates containing relatively rare 3-*O*-sulfated glucosamine residues. To expand the “3-*O*-sulfate proteome,” affinity matrices were created from Chinese hamster ovary (CHO) cell heparan sulfate engineered *in vitro* with and without 3-*O*-sulfate groups. Fractionation of different animal sera yielded several proteins that bound specifically to columns containing 3-*O*-sulfated heparan sulfate modified by two members of the heparan sulfate 3-*O*-sulfotransferase superfamily, Hs3st1 and Hs3st2. Neuropilin-1 was analyzed in detail because it has been implicated in angiogenesis and axon guidance. We show that 3-*O*-sulfation enhanced the binding of neuropilin-1 to heparan sulfate immobilized on plastic plates and to heparan sulfate present on cultured cells.

Chemoenzymatically synthesized 3-*O*-sulfated heparan sulfate dodecamers protected neuropilin-1 from thermal denaturation and inhibited neuropilin-1-dependent, semaphorin-3a-induced growth

*Corresponding Author: Phone: 858-822-1100. Fax: 858-534-5611. jesko@ucsd.edu.

Supporting Information

The Supporting Information is available free of charge on the ACS Publications website at DOI: 10.1021/acscchem-bio.5b00897.

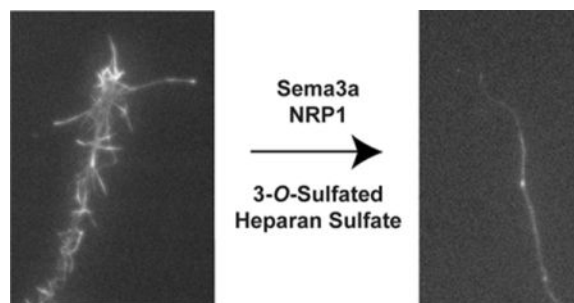
Methods (PDF)
Supporting Table 1 (PDF)
Supporting Table 2 (PDF)
Supporting Table 3 (PDF)
Supporting Figure 1 (PDF)
Supporting Figure 2 (PDF)
Supporting Figure 3 (PDF)

Notes

The authors declare no competing financial interest.

cone collapse of neurons derived from murine dorsal root ganglia. The effect of 3-*O*-sulfation was cell autonomous and specific to Hs3st2 based on collapse assays of neurons derived from Hs3st1- and Hs3st2-deficient mice. Finally, 3-*O*-sulfated heparan sulfate enhanced the inhibition of endothelial cell sprouting by exogenous heparan sulfate. These findings demonstrate a reliable method to identify members of the 3-*O*-sulfate proteome and that 3-*O*-sulfation of heparan sulfate can modulate axonal growth cone collapse and endothelial cell sprouting.

Graphical abstract



Heparan sulfate is a polysulfated glycosaminoglycan found covalently attached to a small number of proteoglycan core proteins at the cell surface and in the extracellular matrix. Its high negative charge allows it to bind and influence the activity of numerous extracellular proteins, resulting in profound effects on cell proliferation, cell differentiation, developmental patterning, regeneration, hemostasis, lipid metabolism, immunity, and inflammation.¹ To a large extent, binding of proteins depends on electrostatic interactions between negatively charged sulfate and carboxyl groups in the glycosaminoglycan with basic amino acid residues in the protein. The affinity of the interaction often depends on the degree of sulfation or specific subsets of sulfate groups. A small number of proteins require a specific spatial arrangement of the sulfate groups and uronic acids for selective, high affinity binding.²

The arrangement of sulfate groups and uronic acid epimers along the chain depends on the action of various enzymes that act during the assembly process, including four *N*-acetylglucosamine *N*-deacetylase-*N*-sulfotransferases, three glucosaminyl 6-*O*-sulfotransferases, a uronyl 2-*O*-sulfotransferase, and a uronyl C5-epimerase.³ A family of seven heparan sulfate 3-*O*-sulfotransferases (Hs3sts) installs sulfate groups at the C3 position of glucosamine units.⁴ In spite of the large number of Hs3st isozymes, sulfation at the 3-*O* position is relatively rare compared to other modifications (e.g., *N*-sulfation and 6-*O*-sulfation of glucosamine units and epimerization and 2-*O*-sulfation of uronic acids), varying from ~10% of glucosamines in Reichert's membrane heparan sulfate to ~1% of glucosamines in endothelial heparan sulfate to none in Chinese hamster ovary cells. The members of the Hs3st family act late in the biosynthetic pathway and thus depend on prior modification by the other sulfotransferases and epimerase.^{5,6} They also have different substrate specificities, resulting in placement of 3-*O*-sulfates in different structural contexts in the polysaccharide.^{3,4}

Although a very large number of heparan sulfate binding proteins have been described,⁷ few protein ligands have been shown to have a predilection to bind to 3-*O*-sulfated heparan sulfate.⁴ Hs3st1 and Hs3st5 can create sites with high affinity for antithrombin (AT).^{8,9} Binding to AT induces a conformational change and potentiates its protease inhibitory activity by several orders of magnitude, rendering it a powerful anticoagulant. Although heparin has proven an invaluable therapeutic agent for preventing clotting and deep vein thrombosis, the functional significance of AT binding to tissue heparan sulfates remains unclear. Inactivation of *Hs3st1*, the primary 3-*O*-sulfotransferase responsible for the assembly of the AT binding sequence, does not cause disseminated coagulopathy but instead results in genetic background-specific lethality, intrauterine growth retardation, and blindness.¹⁰ The relevant protein–heparan sulfate interactions underlying these phenotypes are unknown. Hs3st2, -3a, -3b, -4, -5, and -6 can create the binding site for the Herpes Simplex Virus 1 glycoprotein D (gD), but presumably 3-*O*-sulfation catalyzed by these enzymes results in sequences that have other functions besides conferring susceptibility to infection.⁴ Other ligands that have been shown to prefer 3-*O*-sulfated heparan sulfate include fibroblast growth factor (FGF)7, the ectodomain of FGF receptor-(FGFR)1, cyclophilin B, and stabilin.^{11–13} Recent studies of kit+ progenitor cells in the salivary gland indicate that 3-*O*-sulfate interactions stabilize FGF10/FGFR2b complexes,¹⁴ and genetic studies in zebrafish suggest that bone morphogenic protein 4 and FGF8 also prefer 3-*O*-sulfated heparan sulfate.^{15,16} 3-*O*-Sulfation modulates various developmental and pathological processes, including stem cell differentiation, ciliogenesis, neuronal targeting, and tumor progression, but the proteins that bind to 3-*O*-sulfated sequences and participate in these processes remain largely unknown.^{15–19}

In this article, we set out to create a general strategy to discover proteins whose binding to heparan sulfate is influenced by 3-*O*-sulfation, i.e., to expand the “3-*O*-sulfate proteome.” We took a classical approach based on affinity chromatography using novel heparan sulfate affinity matrices engineered with and without 3-*O*-sulfate groups. Fractionation of various animal sera led to the identification of several proteins not previously known to prefer 3-*O*-sulfated heparan sulfate, including neuropilin-1 (NRP1), a protein that participates in vasculogenesis and axonal guidance.^{20–22} We validated the importance of 3-*O*-sulfation in NRP1-heparan sulfate interactions in various binding assays and by showing that NRP1-dependent semaphorin-3a (Sema3a)-induced axonal growth cone collapse depends on the action of Hs3st2.

RESULTS AND DISCUSSION

Generation of Affinity Matrices Containing 3-*O*-Sulfated Heparan Sulfate

To discover proteins that exhibit preferential binding to 3-*O*-sulfated heparan sulfate, we developed an affinity chromatography strategy in which heparan sulfate lacking 3-*O*-sulfate groups was modified by recombinant Hs3sts and coupled to chromatography resin (Figure 1a). Initial studies sought a reliable, inexpensive source of heparan sulfate that lacked 3-*O*-sulfation and that would serve as a substrate for Hs3st1 (AT-type) and Hs3st2 (gD-type) as candidate 3-*O*-sulfotransferases. A survey of heparan sulfate from several mouse tissues and various cell lines by mass spectrometry revealed that most sources of heparan sulfate contain

3-*O*-sulfate groups. However, heparan sulfate from Chinese hamster ovary cells (CHO-K1) does not,²³ including heparan sulfate derived from CHO-S cells grown to high density in serum-free suspension culture. Incubation of purified CHO-S heparan sulfate with recombinant Hs3st1 or Hs3st2 resulted in sulfation of the chains, indicating the presence of acceptor sites for these enzymes. Under saturating conditions with respect to enzyme concentration, Hs3st1 and Hs3st2 installed one 3-*O*-sulfate group for every 18 or 19 glucosamine residues, respectively (Figure 1b and c). Size exclusion chromatography indicated that the average chain length was ~15 kDa (Figure 1d); thus the average extent of 3-*O*-sulfation was ~1.6 sulfates per heparan sulfate chain leading to a 7% increase in overall sulfation of the chain given the sulfate content of CHO heparan sulfate (~0.8 sulfates/disaccharide).²⁴ By scaling the sulfotransferase reactions, milligram quantities of 3-*O*-sulfated heparan sulfate were readily prepared.

Digestion with a combination of heparin lyases I, II, and III reduces heparan sulfate to disaccharide components, except for characteristically resistant 3-*O*-sulfate containing tetrasaccharides, which can be detected by liquid chromatography/mass spectrometry.^{25,26} As expected, no 3-*O*-sulfated structures were found in unmodified CHO-S heparan sulfate, although strong signals were evident for several commonly occurring *N*-, 2-*O*-, and 6-*O*-sulfate containing disaccharides (D0S0, D0A6, D2S0, D0S6, D2S6; Figure 1e, upper panel). Digestion of Hs3st1-modified heparan sulfate yielded a tetrasaccharide (D0A6-G0S3) characteristic of AT-type 3-*O*-sulfation (Figure 1e, middle panel).²⁵ Analysis of Hs3st2-modified heparan sulfate produced two gD-type disaccharides (D2S3, D2S9) and two tetrasaccharides (Tetra-A and Tetra-B) typical of gD-type sulfotransferases (Figure 1e, bottom panel).²⁶

We next sought a chromatography resin that would allow high capacity binding with minimal background binding of protein. After multiple trials, we found that cyanogen bromide-activated Sepharose (CNBr-Sepharose) had the highest capacity to immobilize heparan sulfate (Supporting Information Figure 1a) reaching 2.8 mg of heparan sulfate per milliliter of beads (Supporting Information Figure 1b). This density is comparable to the extent of conjugation of commercial heparin-Sepharose (~4 mg mL⁻¹ resin). AT passed over the affinity matrices in a buffer containing 0.2 M NaCl did not bind to unmodified heparan sulfate and appeared in the flow-through fraction (Figure 1f). In contrast, a portion of the input AT bound to resin containing Hs3st1-modified heparan sulfate and eluted with 0.5–1 M NaCl, whereas only a small amount of material bound to Hs3st2-modified heparan sulfate under these conditions. Fibroblast growth factor 2 (FGF2) and the soluble form of the receptor for advanced glycation endproducts (RAGE), which are not known to depend on 3-*O*-sulfation, bound to all three resins to a similar extent (Figure 1f). This finding was expected because the chains are identical except in the domains that underwent 3-*O*-sulfation.

Identification of 3-*O*-Sulfate Dependent Proteins

To explore the utility of the columns for identification of novel binding proteins, we passed equal amounts of human, bovine, or mouse sera in parallel over the three affinity resins (Figure 2a) and washed the columns extensively with buffer containing 0.2 M NaCl to

remove weakly bound proteins and then with 1 M NaCl to elute strongly bound proteins. By silver staining, dozens of protein bands were evident in the high salt eluates, most of which appeared to be equally abundant in material eluted from each of the resins (Figure 2b–d). This result was expected because modification by Hs3st isozymes results in only occasional placement of 3-*O*-sulfate groups, with the remainder of the chain remaining unmodified and identical in all three preparations. One striking difference was a band at ~65 kDa (indicated by the asterisk), which was highly enriched from all three sera fractionated on the Hs3st1-modified matrix and had the same molecular weight as AT. No additional proteins were detected by silver staining after washing the columns with 2 M NaCl. Western blot analysis of the high salt fraction obtained from mouse serum confirmed that AT bound preferentially to the Hs3st1 modified matrix (Figure 2b, lower panel).

Proteomic analysis of the material eluted with 1 M NaCl led to the identification of numerous proteins. The analysis was repeated multiple times using bovine (Supporting Information Table 1), mouse (Supporting Information Table 2), and human (Supporting Information Table 3) sera. Each sample yielded hundreds of peptides corresponding to 43–175 distinct proteins, dependent on the source of serum. About half of the eluted proteins from human serum were known heparin/heparan-sulfate-binding proteins (Supporting Information Table 3);⁷ the remainder may be novel heparan sulfate binding proteins. As expected, peptides attributed to AT were enriched 5- to 51-fold in the eluates from Hs3st1-modified resins compared to the control resin (Table 1).

A number of other proteins showed preferential enrichment on the 3-*O*-sulfated resins, based on spectral density of diagnostic peptides and a criterion of minimal enrichment by at least 2.5-fold across multiple analyses. Both proteins of high and low abundance were considered as potential candidates as long as they were enriched on the 3-*O*-sulfated matrices. In this manner, we identified 12 novel 3-*O*-sulfate-dependent candidate proteins (Table 1). Six of these proteins are known heparin/heparan sulfate binding proteins, including amyloid beta A4, biglycan, clusterin, hyaluronan binding protein 2 (HABP2), mannose-binding protein C, and neuropilin-1 (NRP1).⁷ However, their preference for 3-*O*-sulfated heparan sulfate has not been noted previously. Interestingly, these proteins participate in a variety of developmental and physiological processes, including axonal guidance and angiogenesis (NRP1),²⁷ Alzheimer's disease (amyloid beta and clusterin),^{28,29} and coagulation (HABP2 and factors V and XIII).^{30–32} In subsequent studies, we focused on NRP1 to validate affinity fractionation for identifying 3-*O*-sulfate-dependent ligands and to examine the functional implications of 3-*O*-sulfation for binding and biological activity.

NRP1 Interacts Preferentially with 3-O-Sulfated Heparan Sulfate

NRP1 is a type I transmembrane protein with an extracellular region composed of two complementary binding CUB domains (a1 and a2), two coagulation factor domains (b1 and b2), a MAM (meprin, A5, μ) domain (c1), a single membrane-spanning segment, and a short cytoplasmic tail. A heparin-binding site was previously mapped to the b1b2 domain by mutagenesis and demonstrated as essential for oligomerization induced by a mixture of heparin-derived tetradecasaccharides.³³ The binding site, which may extend into the a1–a2 domain,³⁴ provides an electropositive surface potential that measures at least ~40 Å in

length and is long enough to accommodate a tetradecasaccharide.³³ Binding to heparin induces oligomerization presumably by stabilizing the orientation of the b1b2 domains and exposure of an interface for NRP1 dimerization. The NRP1 signaling complex has been proposed to consist of a dimer of trimers containing NRP1/PlexinA/Sema3a in a 2:2:2 ratio based on a crystal structure of the ternary complex.³⁵

To examine the interaction of NRP1 with heparan sulfate, the recombinant human NRP1-b1b2 domain was passed through the affinity columns. NRP1-b1b2 bound poorly to unmodified heparan sulfate, eluting mostly in the flow-through fraction (Figure 2e). In contrast, a large portion of applied material bound to resin containing 3-*O*-sulfated heparan sulfate and eluted at 0.5 M NaCl with a minor portion eluting at 1 M NaCl (Figure 2e). Similar selective binding of intact NRP1 to 3-*O*-sulfated heparan sulfate was noted in serum samples fractionated on the resins (Figure 2f) and after application of recombinant NRP1-b1b2 to heparan sulfates immobilized in 96-well plates (Figure 3a). At saturation, a similar amount of NRP1 bound to both Hs3st1 and Hs3st2 modified heparan sulfate, duplicating the results observed with the affinity resins. Assuming homogeneous single site binding, NRP1 bound to Hs3st1 and Hs3st2 modified heparan sulfate with apparent K_d values of 14.7 nM and 12.4 nM, respectively. In contrast, saturable binding to heparan sulfate without 3-*O*-sulfation did not occur. Similar experiments with AT demonstrated exclusive binding to Hs3st1 modified heparan sulfate with an apparent $K_d = 2.4$ nM (Figure 3b), whereas FGF2 and RAGE bound similarly to all three types of heparan sulfate (Figures 3c and d).

To further investigate the interaction of NRP1 with heparan sulfate, we measured by differential scanning fluorimetry (DSF) the binding of NRP1-b1b2 to chemically defined chemoenzymatically synthesized oligosaccharides. DSF measures the association of a fluorescent dye to hydrophobic domains of proteins exposed by thermal denaturation. An increase in temperature required for denaturation, induced by ligand binding, reflects stabilization of the protein. Two dodecasaccharide ligands were tested (Figure 4a), one that lacks a 3-*O*-sulfate group (1) and a second that contains both an AT-type and a gD-type 3-*O*-sulfate groups (2).³⁶ The overall charge of these oligosaccharides is similar (-16 and -18, respectively). As shown in Figure 4b, the addition of 2 enhanced stabilization versus an unliganded control ($T_m = 1.5$ °C) and relative to the oligosaccharide lacking 3-*O*-sulfate (1; $T_m = 0.7$ °C). In contrast, sucrose octasulfate had no effect on NRP1 thermostability. These data show that NRP1 also preferentially engages 3-*O*-sulfated oligosaccharides in solution.

Finally, we examined binding of NRP1-b1b2 to heparan sulfates expressed as proteoglycans on the surface of animal cells. Under these conditions, NRP1-b1b2 bound to wildtype CHO-K1 cells with an apparent K_d of 230 nM. Transfection of the cells with Hs3st1 or Hs3st2 enhanced binding, yielding apparent K_d values of 125 nM and 37 nM, respectively (Figure 5a). Control experiments showed preferential binding of AT to cells expressing Hs3st1, whereas FGF2 bound to all three cell lines independently of 3-*O*-sulfation (Figures 5b and c). In all cases, binding was dependent on heparan sulfate based on inhibition by heparin lyase digestion or lack of binding to a mutant CHO line lacking heparan sulfate³⁷ (pgsD; Figures 5c and d). NRP1-b1b2 also bound to HeLa cells, which express *HS3ST1*, *HS3ST3A1*, *HS3ST3B1*, and *HS3ST4* (Supporting Information Figure 2). Binding also depended on 3-*O*-sulfation based on a partial loss of binding after shRNA silencing of

HS3ST3A1 (Figure 5e). The ability of NRP1-b1b2 to bind to heparan sulfate expressed on cells (Figure 5) but not to immobilized heparan sulfate (Figure 3) may reflect differences in the way the heparan sulfate chains are presented. Nevertheless, all of the binding assays demonstrate a preference of NRP1 for 3-*O*-sulfated heparan sulfate.

3-O-Sulfation Impacts NRP1-dependent Activity

NRP1 is a coreceptor for plexinA expressed by neurons and plays an important role in axonal targeting and growth cone collapse induced by Semaphorin 3a (Sema3a), for example in dorsal root ganglia (DRG) neurons.^{20,21} DRG explants from E13.5 C57Bl/6 mouse embryos express *Nrp1* mRNA²¹ as well three members of the Hs3st family, *Hs3st1*, *Hs3st2*, and *Hs3st5* (Figure 6a). Overnight stimulation of DRG explants with nerve growth factor results in extension of axons from the explant (Figure 6b), and subsequent treatment of the explants with Sema3a induces collapse of the growth cones (Figure 6c). This process depends on NRP1 based on the ability of a monoclonal blocking antibody against the Sema3a-binding site on NRP1 to completely prevent collapse ($P < 0.001$, Figure 6d).³⁸ An equal concentration of a polyclonal blocking antibody against NRP1 also inhibited collapse ($P < 0.001$, Figure 6d). Pretreatment of the explants with heparin lyase III, which cleaves heparan sulfate, reduced the sensitivity of the growth cones to Sema3a ($P < 0.001$, Figure 6e). Inclusion of soluble heparin also attenuated the response of growth cones to Sema3a (Supporting Information Figure 3). Thus, growth cone collapse induced by Sema3a depends on NRP1 and is modulated by heparan sulfate.

To investigate the influence of 3-*O*-sulfation on NRP1-mediated growth cone collapse, we tested as antagonists the two chemoenzymatically synthesized dodecasaccharides described in Figure 4 (1, 2) and a third containing only AT-type 3-*O*-sulfation (3).³⁶ Preincubation of the explants with each of the dodecasaccharides inhibited growth cone collapse, but the two 3-*O*-sulfated dodecasaccharides were much more potent. The IC₅₀ value for the control dodecasaccharide lacking 3-*O*-sulfate (1) was 7.9 $\mu\text{g/mL}$, whereas IC₅₀ values of 2.4 and 0.6 $\mu\text{g/mL}$ were obtained for AT 3-*O* (3) and AT/gD 3-*O* (2) dodecasaccharides, respectively (Figure 6f).

Finally, we tested if genetic reduction of 3-*O*-sulfation affected NRP1-dependent growth cone collapse by derivation of DRGs from *Hs3st2*^{-/-} E13.5 embryos.³⁹ Quantification of Hs3st expression by qPCR confirmed gene dosage-dependent loss of *Hs3st2* expression in DRGs and no compensatory increase in expression of other Hs3sts (Figure 6a). Notably, growth cone collapse was diminished in a gene dosage dependent manner when stimulated by 10 ng/mL Sema3a ($P < 0.05$; Figure 6g). The addition of Sema3a at a higher concentration (30 ng/mL) suppressed the impact of altering *Hs3st2* expression, an effect that also occurs in other systems in which heparan sulfate acts as a coreceptor (e.g., FGF). Interestingly, inactivation of *Hs3st1*^{-/-} did not attenuate growth cone collapse under these conditions, indicating different functional roles for these two genes *in vivo* (Figure 6h). Experiments with DRGs derived from compound *Hs3st1*^{-/-} *Hs3st2*^{-/-} mutants showed no additive effect over inactivation of *Hs3st2*^{-/-} and confirmed this finding (Figure 6i). Hs3st5-deficient mice have not yet been reported.

The enhancing effect of 3-*O*-sulfation on growth cone collapse indicates that expression of *Hs3sts* in the DRG neuron “fine-tunes” the sensitivity of the growth cone to Semaphorin 3A, which is secreted by the surrounding ectoderm during development of the nervous system.⁴⁰ On the basis of the data presented in Figure 6, we suggest that 3-*O*-sulfation in this context enhances the sensitivity of axons to Semaphorin 3A. Under strongly repulsive conditions, i.e. when the growth cone encounters a high concentration of Semaphorin 3A, repulsion becomes independent of 3-*O*-sulfation. However, as the concentration of Semaphorin 3A declines, the presence of the 3-*O*-sulfated heparan sulfate on the neuron would ensure a robust repulsive response. Thus, the heparan sulfate chains might be part of the sensing system that ensures axon regression under conditions of low concentration of repulsive cues. This hypothesis predicts that differences in axonal guidance might occur *in vivo* in the absence of *Hs3st* expression, especially if Semaphorin 3A secretion is reduced, or by simultaneous reduction of *Hs3st5* in addition to *Hs3st2*.

Finally, we also examined the impact of 3-*O*-sulfation on NRP1-dependent VEGF-A endothelial sprouting.⁴¹ Human umbilical vein endothelial cells (HUVEC) express NRP1 and sprout from microcarrier beads in response to VEGF stimulation⁴² to form luminal structures. Heparin added with VEGF to HUVEC cultures inhibited the extent of endothelial sprouting in a dose-dependent manner (Figure 7a, open bars). Heparan sulfate was less potent (Figure 7a, black bars), but the inhibitory effect was enhanced through 3-*O*-sulfation, in particular by *Hs3st2* (Figure 7a, blue bars). Treatment of the heparan sulfate preparations with heparin lyases prior to addition to the culture medium prevented inhibition (Figure 7b), excluding the possibility that a contaminant was responsible for the inhibition of sprouting.

In summary, we describe a simple technique for identifying novel heparan sulfate-binding proteins. Curiously, many of the candidate proteins that we identified did not exhibit an absolute preference for binding to “AT-type” or “gD-type” 3-*O*-sulfate groups unlike the classic protein ligands, antithrombin and glycoprotein gD, although some bias was noted (Table 1). This finding suggests that some ligands might bind promiscuously to 3-*O*-sulfated sequences, but we cannot exclude the possibility that the conditions used to produce the affinity matrices may contribute to this apparent promiscuity. Comparing the results of studies in CHO cells, DRG neurons, and HUVEC shows that the context in which the 3-*O*-sulfate groups are expressed plays an important role in determining specificity. Nevertheless, the relative ease of producing heparan sulfate in cell culture, the ability to modify its structure enzymatically, and the ease of affinity chromatography expands the toolbox for studying this interesting modification of heparan sulfate.

METHODS

Methods and reagents are described in the Supporting Information.

Statistics

Data analysis was performed using Prism (GraphPad, version 5.0d). Nonlinear regression was used to fit curves and calculate apparent K_d and B_{max} values. *t* tests and ANOVA with *post hoc* tests were used for growth cone collapse assays. *P* values less than 0.05 were considered significant.

Supplementary Material

Refer to Web version on PubMed Central for supplementary material.

Acknowledgments

This work was supported by grants GM93131 and HL107150 (to J.D.E.) and GM094155 (to C.W.V.K.), by training grant T32CA067754 (to B.E.T.) and by F32CA156987 (to E.S) from the National Institutes of Health.

References

1. Sarrazin S, Lamanna WC, Esko JD. Heparan sulfate proteoglycans. *Cold Spring Harbor Perspect Biol.* 2011; 3:a004952.
2. Xu D, Esko JD. Demystifying heparan sulfate-protein interactions. *Annu Rev Biochem.* 2014; 83:129–157. [PubMed: 24606135]
3. Esko JD, Selleck SB. Order out of chaos: Assembly of ligand binding sites in heparan sulfate. *Annu Rev Biochem.* 2002; 71:435–471. [PubMed: 12045103]
4. Thacker BE, Xu D, Lawrence R, Esko JD. Heparan sulfate 3-*O*-sulfation: A rare modification in search of a function. *Matrix Biol.* 2013; 35:60–72. [PubMed: 24361527]
5. Shworak NW, Fritze LMS, Liu J, Butler LD, Rosenberg RD. Cell-free synthesis of anticoagulant heparan sulfate reveals a limiting converting activity that modifies an excess precursor pool. *J Biol Chem.* 1996; 271:27063–27071. [PubMed: 8900197]
6. Liu J, Shworak NW, Sinay P, Schwartz JJ, Zhang L, Fritze LM, Rosenberg RD. Expression of heparan sulfate D-glucosaminyl 3-*O*-sulfotransferase isoforms reveals novel substrate specificities. *J Biol Chem.* 1999; 274:5185–5192. [PubMed: 9988768]
7. Ori A, Wilkinson MC, Fernig DG. A systems biology approach for the investigation of the heparin/heparan sulfate interactome. *J Biol Chem.* 2011; 286:19892–19904. [PubMed: 21454685]
8. Shworak NW, Liu J, Fritze LMS, Schwartz JJ, Zhang LJ, Logeart D, Rosenberg RD. Molecular cloning and expression of mouse and human cDNAs encoding heparan sulfate D-glucosaminyl 3-*O*-sulfotransferase. *J Biol Chem.* 1997; 272:28008–28019. [PubMed: 9346953]
9. Chen J, Liu J. Characterization of the structure of antithrombin-binding heparan sulfate generated by heparan sulfate 3-*O*-sulfotransferase 5. *Biochim Biophys Acta, Gen Subj.* 2005; 1725:190–200.
10. HajMohammadi S, Enjyoji K, Princiville M, Christi P, Lech M, Beeler D, Rayburn H, Schwartz JJ, Barzegar S, De Agostini AI, Post MJ, Rosenberg RD, Shworak NW. Normal levels of anticoagulant heparan sulfate are not essential for normal hemostasis. *J Clin Invest.* 2003; 111:989–999. [PubMed: 12671048]
11. McKeehan WL, Wu XC, Kan M. Requirement for anticoagulant heparan sulfate in the fibroblast growth factor receptor complex. *J Biol Chem.* 1999; 274:21511–21514. [PubMed: 10419453]
12. Deligny A, Denys A, Marcant A, Melchior A, Mazurier J, van Kuppevelt TH, Allain F. Synthesis of heparan sulfate with cyclophilin B-binding properties is determined by cell type-specific expression of sulfotransferases. *J Biol Chem.* 2010; 285:1701–1715. [PubMed: 19940140]
13. Pempe EH, Xu Y, Gopalakrishnan S, Liu J, Harris EN. Probing structural selectivity of synthetic heparin binding to stabilin protein receptors. *J Biol Chem.* 2012; 287:20774–20783. [PubMed: 22547069]
14. Patel VN, Lombaert IM, Cowherd SN, Shworak NW, Xu Y, Liu J, Hoffman MP. Hs3st3-Modified Heparan Sulfate Controls KIT+ Progenitor Expansion by Regulating 3-*O*-Sulfotransferases. *Dev Cell.* 2014; 29:662–673. [PubMed: 24960693]
15. Neugebauer JM, Cadwallader AB, Amack JD, Bisgrove BW, Yost HJ. Differential roles for 3-OSTs in the regulation of cilia length and motility. *Development.* 2013; 140:3892–3902. [PubMed: 23946439]
16. Samson SC, Ferrer T, Jou CJ, Sachse FB, Shankaran SS, Shaw RM, Chi NC, Tristani-Firouzi M, Yost HJ. 3-OST-7 regulates BMP-dependent cardiac contraction. *PLoS Biol.* 2013; 11:e1001727. [PubMed: 24311987]

17. Hirano K, Sasaki N, Ichimiya T, Miura T, Van Kuppevelt TH, Nishihara S. 3-O-sulfated heparan sulfate recognized by the antibody HS4C3 contribute to the differentiation of mouse embryonic stem cells via Fas signaling. *PLoS One*. 2012; 7:e43440. [PubMed: 22916262]
18. Teclé E, Diaz-Balzac CA, Bulow HE. Distinct 3-O-sulfated heparan sulfate modification patterns are required for kal-1-dependent neurite branching in a context-dependent manner in *Caenorhabditis elegans*. *G3: Genes, Genomes, Genet*. 2013; 3:541–552.
19. Miyamoto K, Asada K, Fukutomi T, Okochi E, Yagi Y, Hasegawa T, Asahara T, Sugimura T, Ushijima T. Methylation-associated silencing of heparan sulfate D-glucosaminyl 3-O-sulfotransferase-2 (3-OST-2) in human breast, colon, lung and pancreatic cancers. *Oncogene*. 2003; 22:274–280. [PubMed: 12527896]
20. He Z, Tessier-Lavigne M. Neuropilin is a receptor for the axonal chemorepellent Semaphorin III. *Cell*. 1997; 90:739–751. [PubMed: 9288753]
21. Kolodkin AL, Levengood DV, Rowe EG, Tai YT, Giger RJ, Ginty DD. Neuropilin is a semaphorin III receptor. *Cell*. 1997; 90:753–762. [PubMed: 9288754]
22. Kawasaki T, Kitsukawa T, Bekku Y, Matsuda Y, Sanbo M, Yagi T, Fujisawa H. A requirement for neuropilin-1 in embryonic vessel formation. *Development*. 1999; 126:4895–4902. [PubMed: 10518505]
23. Zhang LJ, Beeler DL, Lawrence R, Lech M, Liu J, Davis JC, Shriver Z, Sasisekharan R, Rosenberg RD. 6-O-sulfotransferase-1 represents a critical enzyme in the anticoagulant heparan sulfate biosynthetic pathway. *J Biol Chem*. 2001; 276:42311–42321. [PubMed: 11551899]
24. Lawrence R, Olson SK, Steele RE, Wang L, Warrior R, Cummings RD, Esko JD. Evolutionary differences in glycosaminoglycan fine structure detected by quantitative glycan reductive isotope labeling. *J Biol Chem*. 2008; 283:33674–33684. [PubMed: 18818196]
25. Yamada S, Yoshida K, Sugiura M, Sugahara K, Khoo KH, Morris HR, Dell A. Structural studies on the bacterial lyase-resistant tetrasaccharides derived from the antithrombin III-binding of porcine intestinal heparin. *J Biol Chem*. 1993; 268:4780–4787. [PubMed: 8444855]
26. Lawrence R, Yabe T, Hajmohammadi S, Rhodes J, McNeely M, Liu J, Lamperti ED, Toselli PA, Lech M, Spear PG, Rosenberg RD, Shworak NW. The principal neuronal gD-type 3-O-sulfotransferases and their products in central and peripheral nervous system tissues. *Matrix Biol*. 2007; 26:442–455. [PubMed: 17482450]
27. Guo HF, Vander Kooi CW. Neuropilin functions as an essential cell surface receptor. *J Biol Chem*. 2015; 290:29120–29126. [PubMed: 26451046]
28. Masters CL, Simms G, Weinman NA, Multhaup G, McDonald BL, Beyreuther K. Amyloid plaque core protein in Alzheimer disease and Down syndrome. *Proc Natl Acad Sci U S A*. 1985; 82:4245–4249. [PubMed: 3159021]
29. Narayan P, Orte A, Clarke RW, Bolognesi B, Hook S, Ganzinger KA, Meehan S, Wilson MR, Dobson CM, Klenerman D. The extracellular chaperone clusterin sequesters oligomeric forms of the amyloid-beta(1–40) peptide. *Nat Struct Mol Biol*. 2012; 19:79–83.
30. Nesheim ME, Taswell JB, Mann KG. The contribution of bovine Factor V and Factor Va to the activity of prothrombinase. *J Biol Chem*. 1979; 254:10952–10962. [PubMed: 500617]
31. Ariens RA, Lai TS, Weisel JW, Greenberg CS, Grant PJ. Role of factor XIII in fibrin clot formation and effects of genetic polymorphisms. *Blood*. 2002; 100:743–754. [PubMed: 12130481]
32. Etscheid M, Hunfeld A, König H, Seitz R, Dodt J. Activation of proPHBSP, the zymogen of a plasma hyaluronan binding serine protease, by an intermolecular autocatalytic mechanism. *Biol Chem*. 2000; 381:1223–1231. [PubMed: 11209757]
33. Vander Kooi CW, Jusino MA, Perman B, Neau DB, Bellamy HD, Leahy DJ. Structural basis for ligand and heparin binding to neuropilin B domains. *Proc Natl Acad Sci U S A*. 2007; 104:6152–6157. [PubMed: 17405859]
34. Uniewicz KA, Ori A, Ahmed YA, Yates EA, Fernig DG. Characterisation of the interaction of neuropilin-1 with heparin and a heparan sulfate mimetic library of heparin-derived sugars. *PeerJ*. 2014; 2:e461. [PubMed: 25024924]
35. Janssen BJ, Malinauskas T, Weir GA, Cader MZ, Siebold C, Jones EY. Neuropilins lock secreted semaphorins onto plexins in a ternary signaling complex. *Nat Struct Mol Biol*. 2012; 19:1293–1299. [PubMed: 23104057]

36. Xu Y, Cai C, Chandarajoti K, Hsieh PH, Li L, Pham TQ, Sparkenbaugh EM, Sheng J, Key NS, Pawlinski R, Harris EN, Linhardt RJ, Liu J. Homogeneous low-molecular-weight heparins with reversible anticoagulant activity. *Nat Chem Biol.* 2014; 10:248–250. [PubMed: 24561662]
37. Lidholt K, Weinke JL, Kiser CS, Lugenwa FN, Bame KJ, Cheifetz S, Massagué J, Lindahl U, Esko JD. A single mutation affects both N-acetylglucosaminyltransferase and glucuronosyltransferase activities in a Chinese hamster ovary cell mutant defective in heparan sulfate biosynthesis. *Proc Natl Acad Sci U S A.* 1992; 89:2267–2271. [PubMed: 1532254]
38. Pan Q, Chanthery Y, Liang WC, Stawicki S, Mak J, Rathore N, Tong RK, Kowalski J, Yee SF, Pacheco G, Ross S, Cheng Z, Le Couter J, Plowman G, Peale F, Koch AW, Wu Y, Bagri A, Tessier-Lavigne M, Watts RJ. Blocking neuropilin-1 function has an additive effect with anti-VEGF to inhibit tumor growth. *Cancer Cell.* 2007; 11:53–67. [PubMed: 17222790]
39. Hasegawa H, Wang F. Visualizing mechanosensory endings of TrkC-expressing neurons in HS3ST-2-hPLAP mice. *J Comp Neurol.* 2008; 511:543–556. [PubMed: 18839409]
40. Nakamura F, Kalb RG, Strittmatter SM. Molecular basis of semaphorin-mediated axon guidance. *J Neurobiol.* 2000; 44:219–229. [PubMed: 10934324]
41. Neufeld G, Cohen T, Shraga N, Lange T, Kessler O, Herzog Y. The neuropilins: multifunctional semaphorin and VEGF receptors that modulate axon guidance and angiogenesis. *Trends Cardiovasc Med.* 2002; 12:13–19. [PubMed: 11796239]
42. Nakatsu MN, Sainson RC, Aoto JN, Taylor KL, Aitkenhead M, Perez-del-Pulgar S, Carpenter PM, Hughes CC. Angiogenic sprouting and capillary lumen formation modeled by human umbilical vein endothelial cells (HUVEC) in fibrin gels: the role of fibroblasts and Angiopoietin-1. *Microvasc Res.* 2003; 66:102–112. [PubMed: 12935768]
43. Wasteson A. A method for the determination of the molecular weight and molecular-weight distribution of chondroitin sulphate. *J Chromatogr.* 1971; 59:87–97. [PubMed: 5110295]
44. Lawrence R, Lu H, Rosenberg RD, Esko JD, Zhang L. Disaccharide structure code for the easy representation of constituent oligosaccharides from glycosaminoglycans. *Nat Methods.* 2008; 5:291–292. [PubMed: 18376390]

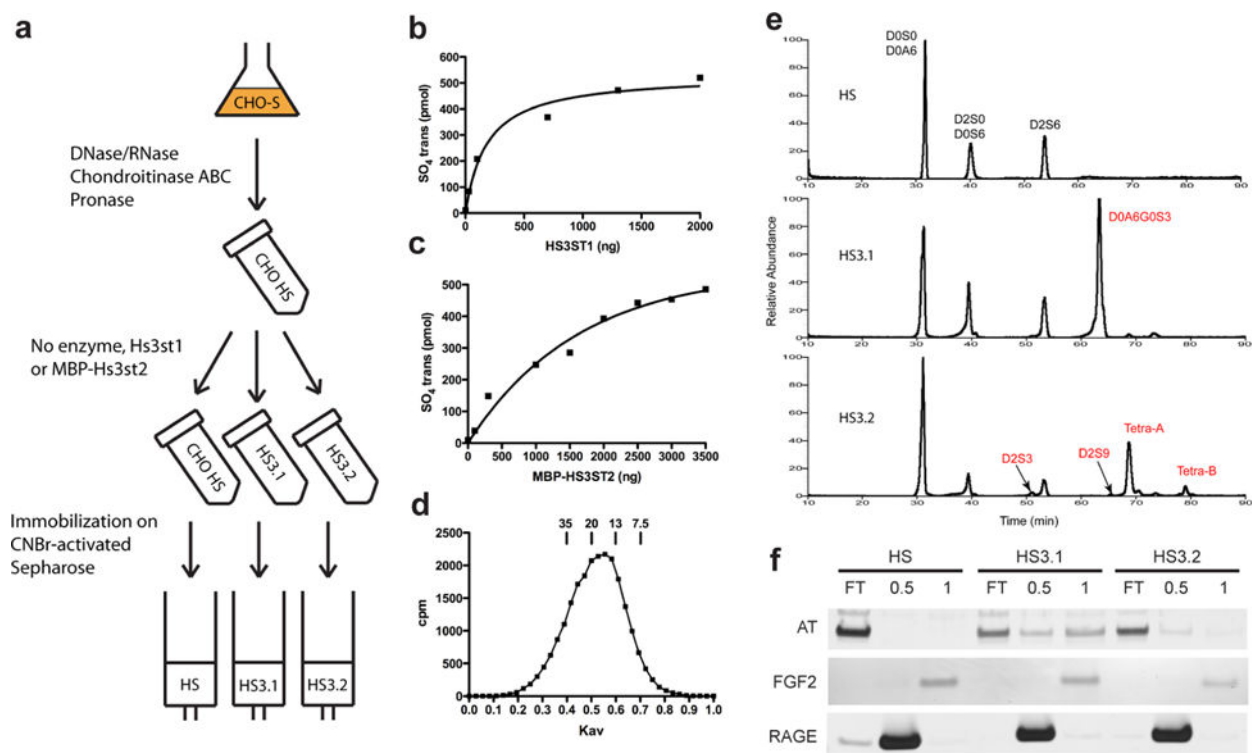


Figure 1.

Construction and validation of 3-*O*-sulfated heparan sulfate affinity matrices. (a) Production scheme of affinity matrices containing Hs3st1 (HS3.1) or Hs3st2 (HS3.2) modified heparan sulfate from CHO-S conditioned medium. (b,c) Modification of CHO-S heparan sulfate by recombinant Hs3st1 (b) and Hs3st2 (c). The data shown are representative of four independent experiments. (d) Elution of CHO-S [³⁵S]heparan sulfate from Sepharose CL-6B. The molecular weight (kDa) of polysaccharide standards is shown above the graph, as described previously.⁴³ The chromatogram is representative of four independent heparan sulfate preparations. (e) Extracted ion current from LC/MS analysis of heparan lyase digestion products derived from the three preparations of heparan sulfate. Individual disaccharides are designated by the disaccharide structural code.⁴⁴ 3-*O*-sulfated species are labeled in red. (f) Fractionation of AT, FGF2, and RAGE on affinity matrices. The flow through (FT), 0.5, and 1 M NaCl fractions are shown by silver stain. Representative gels are shown.

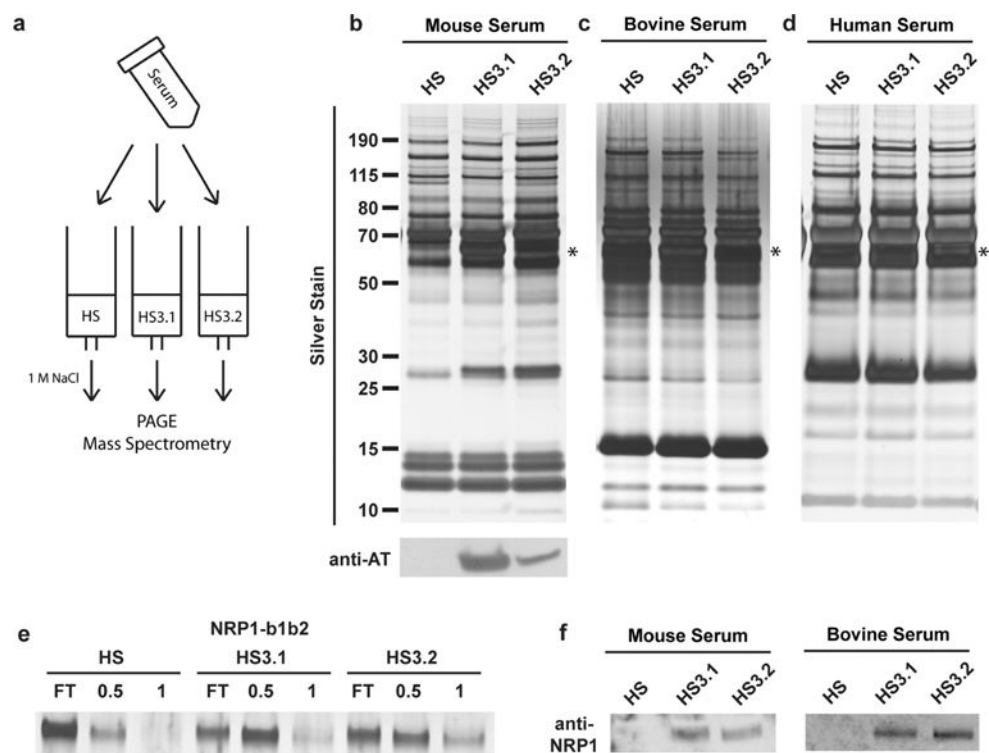


Figure 2. Fractionation of serum on affinity matrices. (a) Work flow for identification of 3-*O*-sulfate-dependent ligands by affinity chromatography. (b,c,d) Elution profile of mouse (b), bovine (c), and human (d) sera from the affinity matrices. An asterisk shows the position of a band enriched on the HS3.1 column and migrating at a position appropriate for AT. Eluates were immunoblotted for AT (b, bottom) and NRP1 (f). Blots are shown with matching silver stains, which serve as the loading control. Representative data are shown from multiple experiments. (e) Elution profile of recombinant human NRP1 from the affinity matrices. The flow through (FT) and eluates (0.5 or 1 M NaCl) are shown. Data shown are representative of three independent experiments.

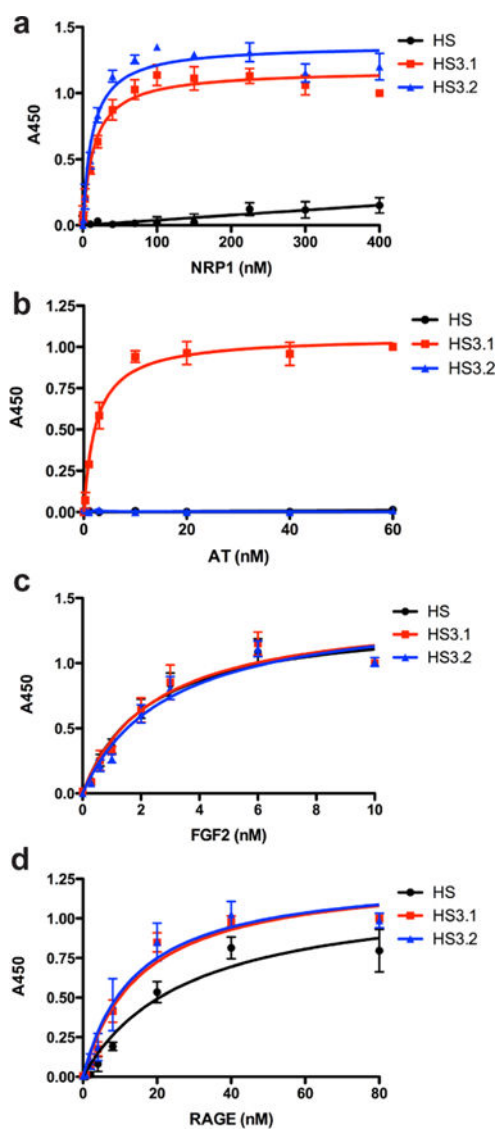


Figure 3. Binding of NRP1 to 3-*O*-sulfated heparan sulfate. NRP1 (a), AT (b), FGF2 (c), or RAGE (d) binding to immobilized heparan sulfate. The data were analyzed by fitting the curves assuming a single binding site. The data shown are the average values from three independent experiments \pm SEM.

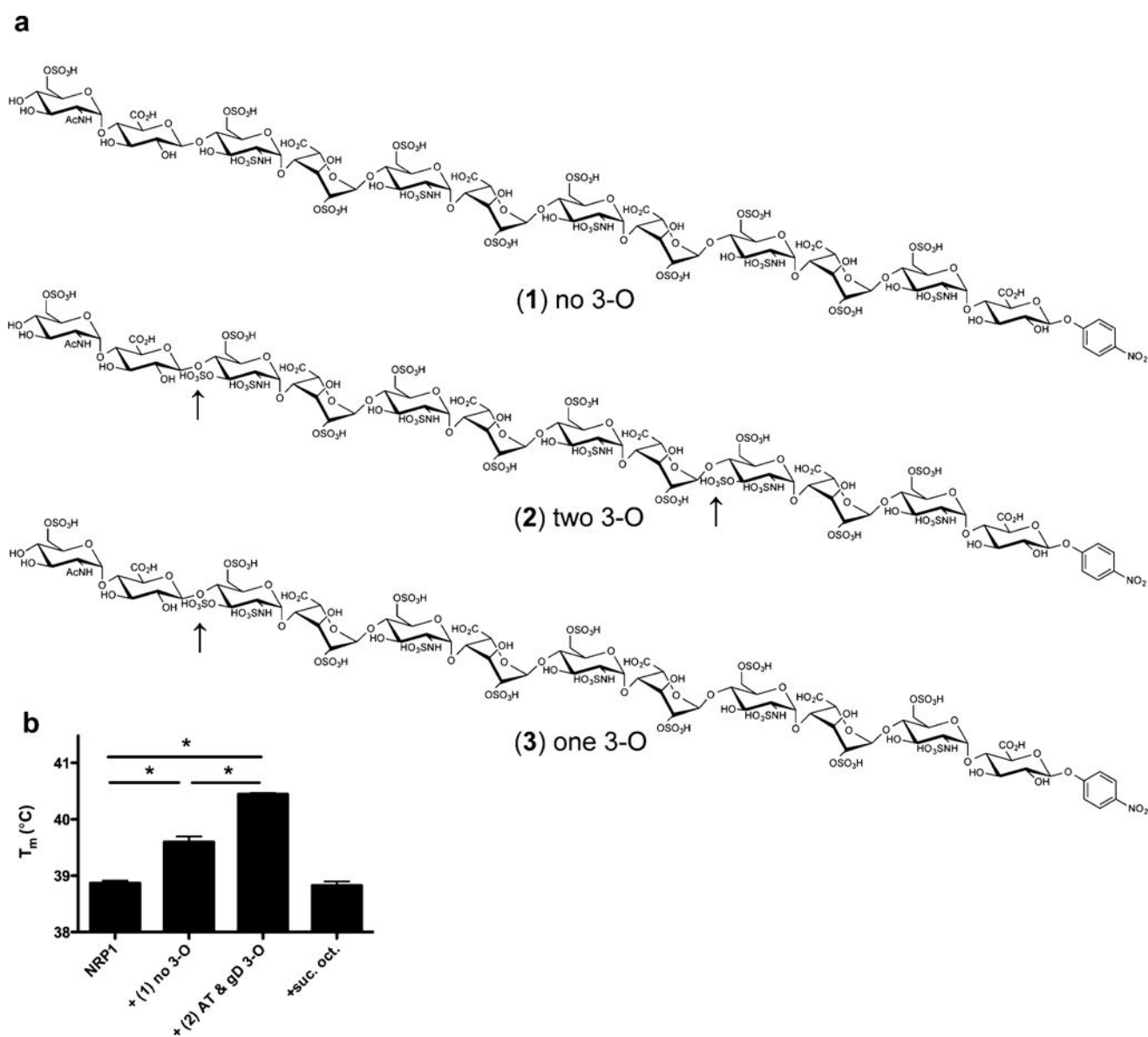


Figure 4. Synthetic 3-*O*-sulfated oligosaccharides. (a) Defined dodecasaccharides produced by chemoenzymatic synthesis.³⁶ The three oligosaccharides are identical except for 3-*O*-sulfate groups (indicated by arrows). (b) Differential scanning fluorimetry of NRP1 incubated with 3-*O*-sulfated oligosaccharides. Incubation of NRP1 with sucrose octasulfate (suc. oct.) served as a control. The mean \pm SD of three replicates is reported (* P < 0.05 by one-way ANOVA with *post hoc* tests).

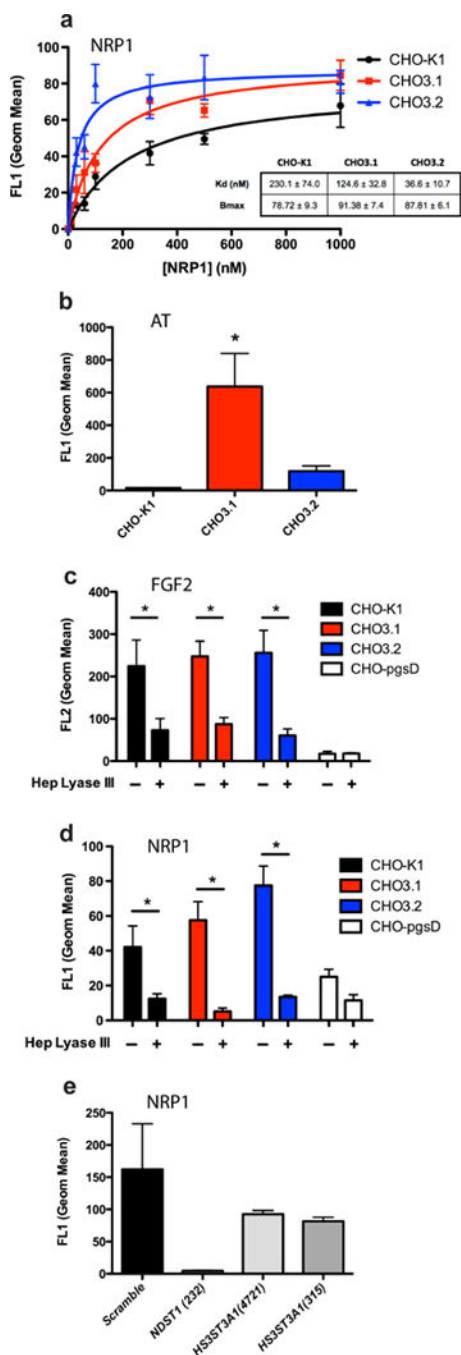


Figure 5. Binding of NPR1 to the cell surface. (a) Binding of NPR1 to CHO-K1, Hs3st1-transduced (CHO3.1), and Hs3st2-transduced (CHO3.2) CHO cells. The apparent K_d and B_{max} were calculated by fitting the data to a single saturable site, and the values are shown in the inset table \pm SEM ($n = 4$). (b) Binding of 100 nM AT to CHO cell surface ($n = 3$; $*P < 0.05$ by one-way ANOVA with *post hoc* tests). (c,d) Binding of ~ 1 nM FGF2 (c) or 300 nM NRP1 (d) to CHO cell surface after treatment with heparin lyase III or to CHO-pgsD cells ($n = 3$, $*P < 0.05$ by *t* test). (e) Binding of 300 nM NRP1 to the HeLa cell surface. shRNA

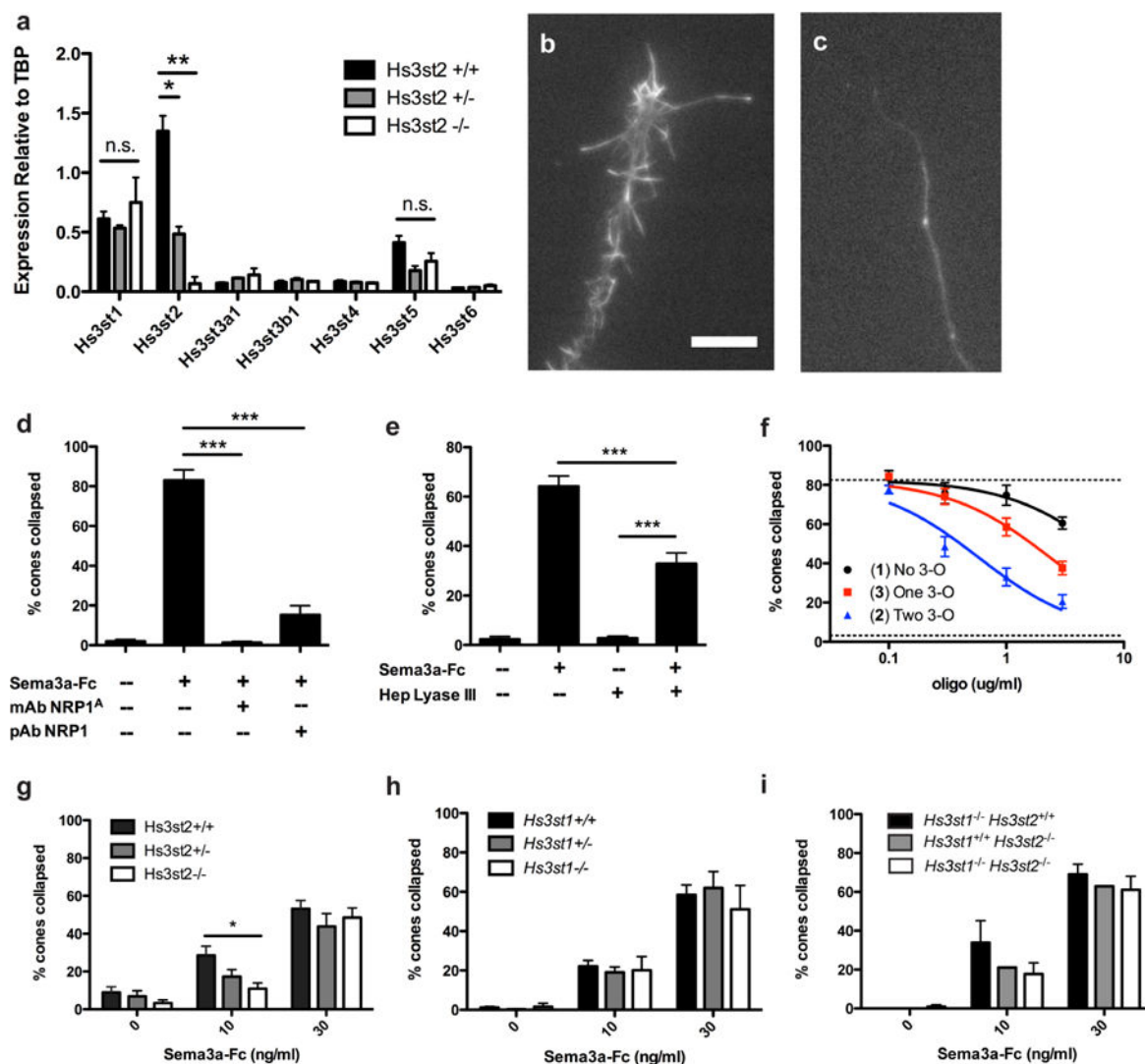
mediated knockdown was performed on heparan sulfate sulfotransferases (*NDST1* and *HS3ST3A1*). Data represent duplicate measurements from two experiments.

Author Manuscript

Author Manuscript

Author Manuscript

Author Manuscript

**Figure 6.**

Axonal growth cone collapse modulated by 3-*O*-sulfation. (a) Expression of Hs3sts in mouse E13.5 dorsal root ganglion. E13.5 DRG were dissected from six mouse embryos of each genotype and *Hs3st* expression was analyzed by qRT-PCR. The average values are shown \pm SEM ($n = 3$; * $P < 0.05$, ** $P < 0.01$ by one-way ANOVA and *post hoc* tests). (b,c) Representative images of growth cones from E13.5 DRG explants before (b) and after (c) Semaphorin 3A-induced collapse. Scale bar is 10 μ m. (d) Effect of NRP1 monoclonal and polyclonal blocking antibodies (10 μ g mL⁻¹) on growth cone collapse induced by Semaphorin 3A (30 ng mL⁻¹). The values shown represent the average \pm SEM ($n = 3$; *** $P < 0.001$ by one-way ANOVA and *post hoc* tests). (e) Heparin lyase III treatment of cell surface heparan sulfate in growth cone collapse with Semaphorin 3A (30 ng mL⁻¹). The values shown represent the average \pm SEM ($n = 3$; *** $P < 0.001$ by one-way ANOVA and *post hoc* tests). (f) Effect of dodecasaccharides on Semaphorin 3A (30 ng mL⁻¹) induced growth cone collapse. Dashed lines represent the extent of growth cone collapse stimulated by Semaphorin 3A in the absence of oligosaccharides (top) and in the absence of Semaphorin 3A (bottom). Data shown are the average

of two separate experiments performed in triplicate. (g) Sema3a-induced growth cone collapse in DRG from *Hs3st2*^{+/+} ($n = 9$), *Hs3st2*^{+/-} ($n = 11$), and *Hs3st2*^{-/-} ($n = 10$) embryos. (h) Sema3a-induced growth cone collapse in DRG from *Hs3st1*^{+/+} ($n = 5$), *Hs3st1*^{+/-} ($n = 10$), and *Hs3st1*^{-/-} ($n = 2$) embryos. Data from multiple litters, each of which had embryos of each genotype, were compiled to create the final data set shown in g and h. The differences between the genotypes were statistically significant by one-way ANOVA and *post hoc* tests ($*P < 0.05$). (i) Compounding mutations in *Hs3st1* and *Hs3st2* ($n = 4$) had no additive effect on growth cone collapse.

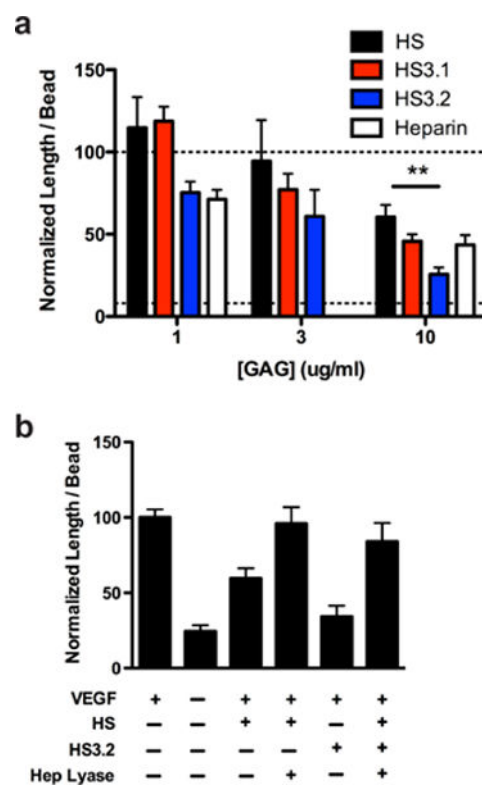


Figure 7. Endothelial cell sprouting modulated by 3-*O*-sulfation. (a) Effect of soluble heparan sulfate or heparin on VEGF-induced endothelial cell sprouting. The values shown represent the average \pm SEM ($n = 2-4$, $**P < 0.01$ by one-way ANOVA and *post hoc* tests). The dotted lines show the extent of sprouting in the absence of added heparan sulfate (top) and in the absence of VEGF (bottom). (b) Degradation of heparan sulfate destroys the inhibitory activity of exogenous heparan sulfate. The values shown represent the average \pm SEM ($n = 5-6$).

Table 1
Spectral Density of Serum 3-O-Sulfate Dependent Candidate Proteins in Affinity Matrix Eluates^a

protein name	bovine 1			bovine 2			mouse 1			mouse 2			human 1		
	HS	HS3.1	HS	HS3.1	HS3.2	HS	HS	HS3.1	HS3.2	HS	HS3.1	HS3.2	HS	HS3.1	HS
amyloid beta (A4) protein (Q6GGR78)				1 (1.7)	3 (4.5)			1 (1.4)			1 (1.4)				
antithrombin (Q543J5)	1 (1.9)	51 (70.5)	7 (16.1)	37 (49.7)	17 (29.9)	9 (23.9)	4 (8.6)	231 (78.9)			80 (55.5)			28 (40.0)	7 (16.6)
biglycan (Q3TNY9)				6 (23.6)	8 (29.8)						2 (5.1)				
elasterin (Q549A5)		1 (3.6)		2 (6.2)	5 (8.2)	4 (12.1)		3 (8.5)			3 (9.4)			6 (18.8)	1 (5.1)
coagulation factor V (088783)				1 (0.5)	1 (0.6)										4 (2.4)
coagulation factor XIII (Q8BH61)	3 (4.2)	8 (12.6)		2 (3.4)	5 (8.5)									1 (1.2)	
decorin (Q3UKR1)				1 (4.2)	4 (13.3)						1 (4.0)			3 (10.2)	
hyaluronan-binding protein 2 (Q8K0D2)		1 (1.8)		7 (17.7)	13 (25.8)						6 (12.7)			11 (21.9)	1 (1.8)
mannose-binding protein C (P41317)								1 (4.5)		3 (20.5)	1 (4.5)			3 (20.5)	
neuropilin 1 (Q6PAR3)				2 (3.6)	6 (10.9)						1 (1.6)			3 (5.4)	2 (2.9)
putative uncharacterized protein (Q9DBD0)											3 (5.3)			2 (2.9)	
serglycin (P13609)				3 (19.3)	7 (26.0)						14 (38.2)			18 (28.3)	
synaptotagmin-like 4 (Q549X6)											6 (11.1)			3 (5.3)	

^aPeptide counts of 3-O-sulfate dependent candidate proteins in affinity matrix eluates. The compiled results are shown from multiple analyses using bovine, mouse, and human serum. The number of peptides attributed to each protein with greater than 95% confidence is displayed for eluates from affinity matrices. The resulting percentage protein coverage is shown in parentheses. Empty boxes reflect samples with zero peptides identified. The accession number for each protein in the mouse serum is displayed with the protein name.